A Comparative Study of Five SWP Low-Dispersion Correction Algorithms

I. Introduction

The accompanying report (Cassatella et al. 1980) presents an algorithm that can be used to correct low-dispersion SWP spectra processed with the bad Intensity Transfer Function (ITF). That algorithm is called the 3 Agency 4th file method. It consists of a transformation between flux values in the old and the new ITF, a scheme for applying the flux transformation to the spatially-resolved spectra (essr), and a formula for re-extracting the gross and background spectra from the essr file. It was adopted by the three agencies, NASA, ESA, and the SRC, because it is simple, because it is applicable to both extended and point source spectra, and because it is usually more accurate than the inherent photometric accuracy of correctly processed spectra.

Other algorithms exist which differ from this one chiefly in the way the extracted spectra are decomposed to allow the flux transformation to be applied. In this report, we present a comparative study of the accuracy of four other algorithms with the 3 Agency 4th file method. Three of the comparison algorithms also are applied to the spectra from the essr file. They differ from the 3 Agency method in that they use various interpolation methods to attempt to decompose the samples in the essr spectra into approximations of the Flux Number (FN) values of the original pixels. The fourth comparison algorithm applies to the spectra in the merged spectra file (eslo). It assumes the shape of the point spread function to be Gaussian to decompose the net spectrum. In Section II, the alternative algorithms are defined. Section III gives the comparisons of the accuracy of the algorithms.

Some users have developed programs for re-extracting the spectrum from a geometrically and photometrically corrected image (gpi file) that has been corrected by the flux transformation in Cassatella et al. to an approximation of an image processed with the good ITF. These users include M.A.J. Snijders (at University College London) and J. Koornneef and K. deBoer (1979). Such a program should be quite accurate and, additionally, offers the opportunity to improve other aspects of the spectral extraction. However, these programs are much longer and more complicated than the algorithms considered here. The gpi file algorithms will not be discussed further here.

II. Definitions of the Alternative Algorithms

The principal difference in the correction algorithms is the method by which the original pixel values are estimated from the samples present in the extracted spectra. (The transformation given in Section II of Cassatella et al. is strictly valid only for single pixels.) The 3 Agency 4th file method assumes that all the pixels contained in a sample have the same intensity value. The other algorithms discussed here attempt to decompose samples by various means. The three which apply to the essr file use linear, quadratic, and bi-linear interpolation. The fourth, which applies to the eslo file, assumes the point spread function has a Gaussian

shape whose width varies with wavelength.

II.1 The Linear Decomposition Algorithm

This algorithm applies to spectra in the essr file.

Since the sample area in the essr spectra is twice the area of a pixel, the sample may include portions of 4 to 7 pixels. We make the simplifying assumption that each sample contains one whole pixel and one quarter each of four other pixels as shown in Fig. 1. We further assume that, for the correction of the sample J,K, the FN values in pixels b and c are equal and that those in pixels d and e are equal.

To estimate the individual values of pixels a, b, c, d, and e from the summed value in the sample, we use a linear interpolation perpendicular to the direction of the dispersion. Therefore, to correct sample K in order J it is necessary to use the values of the corresponding samples in orders J-1 and J+1. To define the algorithm, let

(2.0)
$$S_{J-1,K} = \text{the FN value of the Kth sample from order (or line) J-1,}$$
$$S_{J,K} = \text{the FN value of the Kth sample from order J,}$$
$$S_{J+1,K} = \text{the FN value of the Kth sample from order J+1,}$$
and $$P_q = \text{the FN value assigned to pixel q by interpolation.}$$

Then the linear decomposition is given by

(2.1)
$$P_{J-\frac{1}{2}} = \tfrac{1}{4}\left[S_{J-1,K}+S_{J,K}\right] = P_b = P_c$$

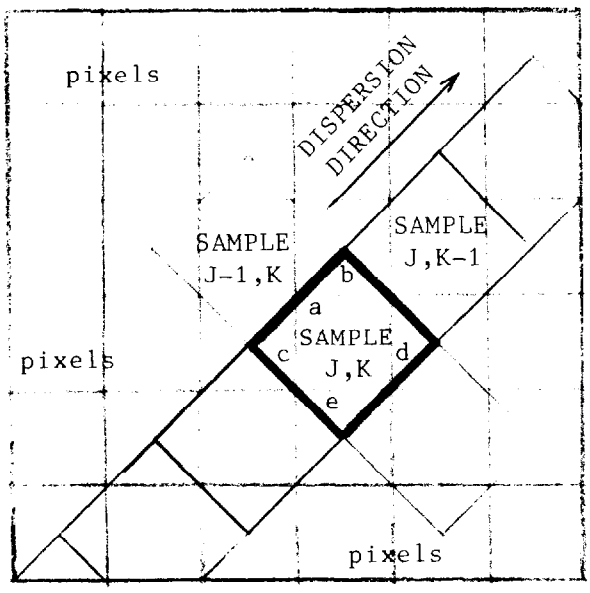

Fig.1 - Extraction slit for the spatially-resolved spectra (essr file). Pixels are indicated by the grid with an oblique dispersion direction. In this simplified view, sample J,K includes all of pixel a, and one-quarter of pixels b, c, d, and e. Sample J,K-1 is in the same order as sample J,K but is at shorter wavelengths. Sample J-1,K is at the same wavelength as sample J,K but in a different order. This geometry is the basis of all the essr decomposition algorithms.

$$P_{J+\frac{1}{2}} = \tfrac{1}{4}[S_{J,K}+S_{J+1,K}]$$
$$= P_d = P_e \quad ,$$

and $$P_a = S_{J,K} - \tfrac{1}{2}[P_{J-\frac{1}{2}}+P_{J+\frac{1}{2}}].$$

After P_a, $P_{J-\frac{1}{2}}$, and $P_{J+\frac{1}{2}}$ are corrected by the flux transformation given in Section II of Cassatella et al., the old (i.e. bad) FN value of the sample is replaced with the sum

$$S_{J,K,corr} = P_{a,corr} + \tfrac{1}{2}[P_{J-\frac{1}{2},corr}+P_{J+\frac{1}{2},corr}] \tag{2.2}$$

where the meaning of "corr" is obvious. Finally, the new gross and background spectra are extracted from the corrected essr file as in the 3 Agency 4th file method.

II.2 The Quadratic Decomposition Algorithm

This algorithm applies to the spectra in the essr file.

This algorithm uses a quadratic interpolation perpendicular to the dispersion to determine values for pixels a, b, c, d, and e. It uses the same assumptions used for the Linear Decomposition algorithm. Using the definitions given in equations 2.0 in Section II.1, the Quadratic Decomposition is defined by

$$P_{J-\frac{1}{2}} = \frac{5}{32}S_{J-1,K} + \frac{7}{16}S_{J,K} - \frac{3}{32}S_{J+1,K}$$
$$= P_b = P_c \quad ,$$

$$P_{J+\frac{1}{2}} = -\frac{3}{32}S_{J-1,K} + \frac{7}{16}S_{J,K} + \frac{5}{32}S_{J+1,K} \tag{2.3}$$
$$= P_d = P_e \quad ,$$

and $$P_a = \frac{9}{16}S_{J,K} - \frac{1}{32}[S_{J-1,K}+S_{J+1,K}] \quad .$$

The FN values, P_a , $P_{J-\frac{1}{2}}$, and $P_{J+\frac{1}{2}}$, are corrected, the sample is reconstructed using equation 2.2, and the spectra are re-extracted as for the Linear Decomposition algorithm.

II.3 The Bi-linear Decomposition Algorithm

This algorithm applies to the spectra in the essr file.

This algorithm differs from the two preceeding algorithms in that the pixels b and c and the pixels d and e are not assumed to be equal. Values are assigned to these pixels by doing a bi-linear interpolation perpendicular and parallel to the dispersion. With the same definitions of symbols used in Section II.1 above, the Bi-linear Decomposition is defined by

$$P_b = \frac{1}{8}\left[S_{J-1,K-1} + S_{J-1,K} + S_{J,K-1} + S_{J,K}\right] ,$$

$$P_c = \frac{1}{8}\left[S_{J-1,K} + S_{J-1,K+1} + S_{J,K} + S_{J,K+1}\right] ,$$

(2.4) $$P_d = \frac{1}{8}\left[S_{J,K-1} + S_{J,K} + S_{J+1,K-1} + S_{J+1,K}\right] ,$$

$$P_e = \frac{1}{8}\left[S_{J,K} + S_{J,K+1} + S_{J+1,K} + S_{J+1,K+1}\right] ,$$

and $$P_a = S_{J,K} - \tfrac{1}{4}\left[P_b + P_c + P_d + P_e\right] .$$

The estimated pixel values are corrected by the standard flux transformation, the new sample value is constructed from the sum

(2.5) $$S_{J,K,corr} = P_{a,corr} + \frac{1}{4}\left[P_{b,corr} + P_{c,corr} + P_{d,corr} + P_{e,corr}\right] ,$$

and the spectra are re-extracted as in the 3 Agency algorithm.

II.4 The Gaussian Decomposition Algorithm

This algorithm applies to point source spectra in the eslo file.

The spectra in the eslo file can be corrected directly if a reasonably accurate method exists for decomposing the spectrum approximately into its component pixels. Koornneef and deBoer (1979) have found that the point spread function is nearly Gaussian for point-source spectra. From additional work, Koornneef (1979) has found that the width of the spectrum is a function of wavelength. His relationship can be expressed as

(2.6) $$\sigma = 0.345 + 4.198E\text{-}4*\lambda$$

where the wavelength is given in Ångstroms and the unit length of σ is $\sqrt{2}$ times the length of the side of a pixel.

Approximate values of the original pixels are found from the formula

(2.7) $$P_j = c_j \, FN_{net,old} + FN_{bkgd,old}$$

where $$c_j = \frac{0.20}{\sigma} \exp\left[-0.5\,(x/\sigma)^2\right],$$

x = the distance perpendicular to the dispersion of the pixel from the peak of the spectrum (in the same units as σ),

$FN_{net,old}$ = the FN value of the sample in the net spectrum,

and $$FN_{bkgd,old} = \left[FN_{gross,old} - FN_{net,old}\right]/17 .$$

In this algorithm, x has the values 0.0, ±0.5, ±1.0, ±1.5, ±2.0, and ±2.5 for the subscript j values of 1 through 11.

The pixel FN values, P_j and $FN_{bkgd,old}$, are corrected by the transformation in Section II of Cassatella et al. The corrected net samples are generated by the equation

$$(2.8) \quad FN_{net,corr} = \sum_{j=1}^{11} w_j P_{j,corr} - FN_{bkgd,corr} \sum_{j=1}^{11} w_j$$

where w_j is a weighting factor intended to compensate for the decomposition not extending to as large distances from the spectrum as the original extraction. To properly normalize the net spectrum, w_j is defined by

$$w_j = 1.0 \qquad \text{for } j=1 \text{ through } j=9$$

$$(2.9) \quad \text{and} \quad w_{10} = w_{11} = \frac{1 - \sum_{j=1}^{9} c_j}{2\, c_{10}} \,.$$

While the Gaussian decomposition can be applied only to point-source spectra and the accuracy of the decomposition may depend on telescope focus and the centering of the spectrum, it has the advantage that it might be used to correct high-dispersion spectra from the eshi file.

III. Comparisons of the Accuracy of the Five Algorithms

The accuracy of the algorithms was tested by applying them to a sample of spectra which had been processed with both the bad and the good ITF as described in Cassatella et al. After being corrected by each algorithm, the bad ITF spectra were divided, sample by sample, by the spectra processed with the good ITF. For the Gaussian Decomposition algorithm, the corrected net was compared with the net from the correctly processed eslo file. For the algorithms which use the essr file, the comparison,good ITF spectra were extracted also from the essr files. In the essr spectral extraction, the background spectrum was filtered with a 21 point median filter and smoothed with a 5 point averaging. Only one spectrum, SWP4316, was taken through the small aperture. All other spectra tested were through the large aperture.

Summaries of the results of this testing are given in Table 1 and Table 2 for point source and for extended and trailed source spectra respectively. The first four columns of both tables give the target name, the image sequence number, the exposure time in minutes, and the background level in FN per pixel. In Table 1, columns 5 and 6 give the reproducibility and linearity errors which appeared in Table 3 of Cassatella et al. The remaining columns both

TABLE 1

THE ACCURACY OF THE CORRECTION ALGORITHMS ON POINT SOURCE SPECTRA

TARGET	IMAGE	EXP TIME	BKGD/PIXEL	INTRINSIC ERROR		CORRECTION ERRORS									
						3 AGENCY		LINEAR		QUADRATIC		BI-LINEAR		GAUSSIAN	
				MEAN	RMS	MEAN	RMS	MEAN	RMS	MEAN	RMS	MEAN	RMS	MEAN	RMS
+28°4211	SWP2139	0.43 min	-38	-	-	-1.5%	1.8%	-0.2%	1.5%	-0.6%	1.3%	-0.3%	1.5%	+1.8%	2.4%
	SWP2138*	0.28	3490	-5.5%	17.4%	+0.7	1.4	+0.0	1.4	+0.2	1.3	-0.1	1.3	+0.2	2.1
HD 60753	SWP4315	0.17	-169	-	-	-0.6	2.7	-0.5	1.8	-0.5	1.6	-0.6	1.8	+0.2	1.9
	SWP6823	0.17	-102	-	-	-0.5	2.0	-0.4	1.5	-0.5	1.3	-0.5	1.5	+1.0	2.0
	SWP6826	0.08	-109	-1.8	7.2	-1.2	3.0	+0.2	2.5	-0.9	2.0	+0.2	3.9	-0.6	2.8
	SWP6824*	0.08	2118	-5.0	10.7	+2.2	3.1	+2.1	2.9	+2.3	3.0	+1.9	2.9	+6.5	5.7
	SWP6825*	0.08	5536	+5.8	21.2	-0.4	0.6	-0.4	0.7	-0.4	0.6	-0.4	0.7	-0.6	0.6
+33°2642	SWP4003	4.00	-30	-	-	-0.8	2.0	-0.4	1.3	-0.5	1.2	-0.5	1.4	+1.3	2.5
	SWP4006	2.00	0	-3.1	7.3	+0.3	2.7	+1.0	2.7	-0.4	2.1	+0.9	2.8	-0.2	3.0
	SWP4007	1.20	33	-4.2	9.1	-0.6	3.2	+0.0	1.9	-0.4	2.2	-0.2	2.1	+0.8	2.8
	SWP4004*	0.40	-	-19.6	16.0	+0.4	3.8	+0.5	3.8	+0.3	3.8	+0.1	3.8	+0.5	5.0
	SWP4005*	0.40	-	-15.7	28.6	-0.1	5.8	-0.0	5.8	-0.4	6.0	-0.7	6.1	+0.5	7.4
ζ Cas	SWP4316	0.02	71	-	-	-0.4	1.5	+0.0	1.4	+0.0	1.2	-0.0	1.5	+0.6	1.3
Capella	SWP4626*	0.67	-62	-	-	-0.2	1.5	+0.1	1.3	-0.2	1.7	-0.3	1.5	+0.4	1.7
SMC X-1	SWP6219	37	90	-	-	-0.6	2.0	-0.3	1.5	-0.3	1.1	-0.3	1.5	-0.9	1.5
CI Cyg	SWP5485	45	110	-	-	+0.4	2.7	+0.2	2.1	+0.3	2.4	+0.0	2.0	-0.6	2.8
U Sco	SWP5728	40	108	-	-	+0.1	2.8	+0.8	2.6	-0.2	2.2	+0.8	2.8	-0.5	3.3
LMC X-4	SWP6220	45	152	-	-	-0.1	1.9	-0.2	1.4	-0.4	1.2	-0.2	1.4	-1.9	2.5
V603 Aql	SWP5921	15	160	-	-	-1.2	1.9	-1.0	1.3	-0.5	1.2	-1.0	1.5	-1.5	1.9
HR Del	SWP5918	20	180	-	-	-1.3	2.1	-0.8	1.6	-0.4	1.6	-0.8	1.3	-1.2	3.2
RU Lup	SWP5569*	180	985	-	-	-4.3	3.1	-3.0	2.8	-3.2	3.0	-2.9	3.1	-	-
0837-120	SWP4292	392	3200	-	-	-1.6	6.4	-1.7	6.3	-1.6	6.4	-2.1	6.7	+0.2	6.8

* Errors calculated after regions around one or two discrepant points excluded. See text.

TABLE 2

THE ACCURACY OF THE CORRECTION ALGORITHMS ON EXTENDED AND TRAILED SOURCE SPECTRA

TARGET	IMAGE	EXP TIME	BKGD/PIXEL	CORRECTION ERRORS							
				3 AGENCY		LINEAR		QUADRATIC		BI-LINEAR	
				MEAN	RMS	MEAN	RMS	MEAN	RMS	MEAN	RMS
HD 60753	SWP3223	0.41 min	-	-0.2%	0.8%	+0.0%	0.7%	+0.1%	0.6%	-0.1%	0.7%
	SWP3220	0.34	-	-0.6	1.0	+0.1	0.8	-0.2	0.9	-0.2	0.8
	SWP3221	0.27	-	-0.5	1.0	-0.2	1.0	-0.3	1.0	-0.2	1.2
	SWP3222	0.20	-	-0.2	1.3	-0.1	1.2	-0.3	1.3	-0.1	1.2
η UMa	SWP2341	0.005	-	-0.3	0.8	-0.2	0.7	-0.2	0.7	-0.3	0.6
NGC 6093	SWP6026	95	481	+2.0	3.6	+1.6	3.2	+1.7	3.4	+1.4	2.8
N 63 A	SWP3490	395	2800	+0.0	0.6	-0.3	0.6	-0.2	0.6	-0.4	0.6
N 49	SWP2115*	385	2840	+0.3	5.7	+0.3	5.6	+0.3	5.7	+0.4	5.3

* Errors calculated after regions around one discrepant point excluded. See text.

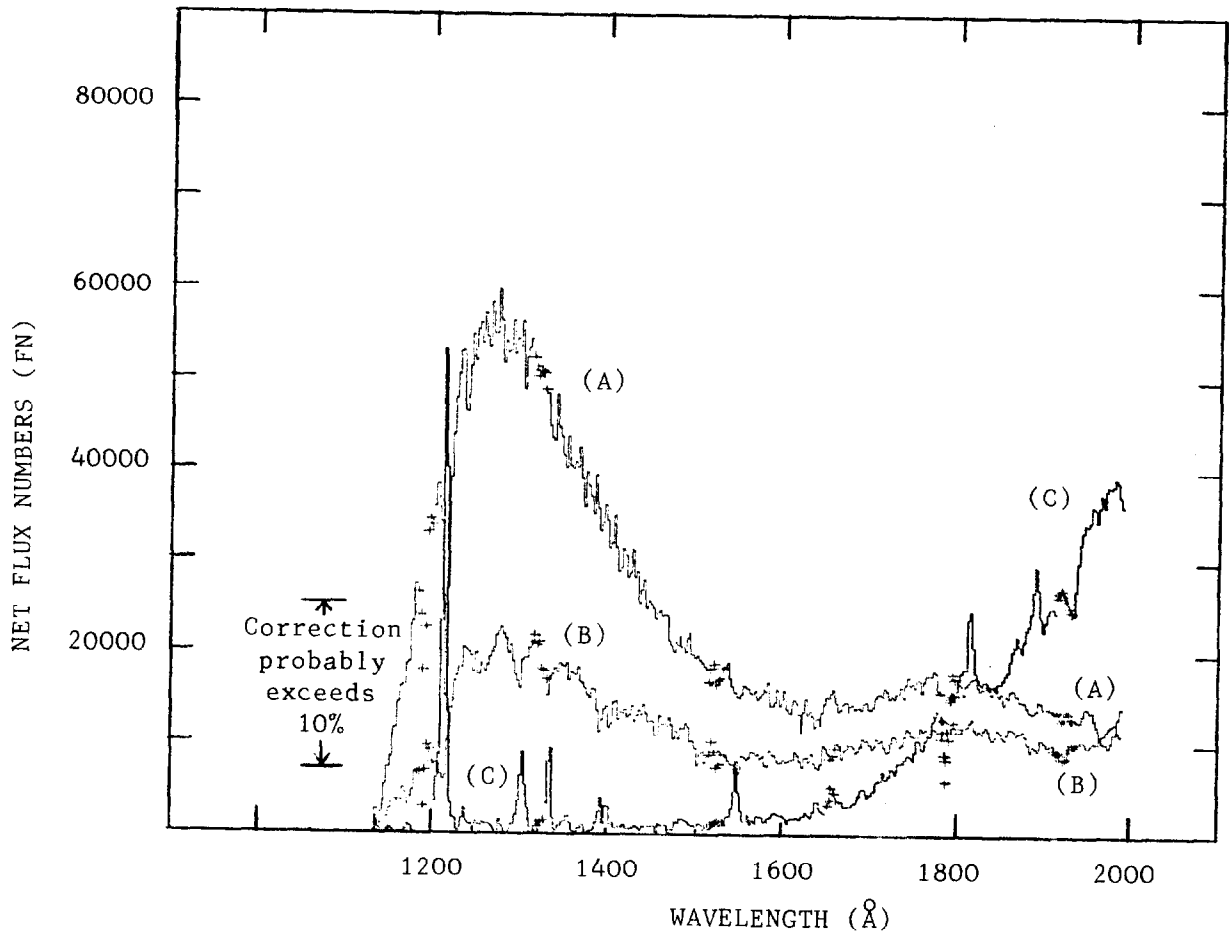

Fig.2- The large aperture Net spectra derived from images (A) SWP2139 of BD+28°4211, (B) SWP4006 of BD+33°2642, and (C) SWP4626 of Capella. The interval of FN where the correction is expected to be greater than 10% is indicated.

in Table 1 and in Table 2 give the mean errors and the RMS errors for the correction algorithms when applied to each of the spectra.

The correction errors given here are defined by

$$100 \times \left[\frac{FN_{net,corr} - FN_{net,reprocessed}}{FN_{net,reprocessed}} \right] .$$

The mean and RMS errors for most of the spectra were derived for an 800 Å band centered on 1550 Å. One group of errors which deviates from this rule are those given for the Gaussian algorithm for spectra SWP6219 through SWP4292 in Table 1. These errors were determined by Cassatella and Ponz (1979) and refer to a 600 Å band centered on 1550 Å. The other group which deviates from the rule are the eight spectra marked by asterisks. For these spectra, one or two deviant points greatly affected the RMS error and, to a lesser extent, the mean error. The deviant points in seven of the spectra correspond to the reseaux in the spectrum at 1190 Å and at 1790 Å. The deviant point in the eighth spectrum occurs where where the flux in the net reprocessed spectrum is near zero. We judged that discarding the deviant points in these spectra would be justifiable. Accordingly, the errors were recalculated with the 50 Å band containing the deviant point excluded. The recalculated errors for these eight spectra are much lower in this report than the original errors given in Cassatella et al.

To aid the user in evaluating the summarized statistics, correction errors as a function of wavelength are shown in Fig. 3,4, and 5 for three spectra. The net spectra for these three are shown in Fig. 2. One (SWP2139) is a well exposed spectrum of BD+28°4211, one (SWP4006) is an underexposed spectrum of BD+33°2642, and the last (SWP4626) is a spectrum of Capella. The zone in FN in which the correction to the incorrectly processed spectrum probably exceeds 10% is also indicated in Fig. 2. It can be seen that this zone contains nearly all of SWP4006, about 60% of SWP2139, and much of the continuum in SWP4626.

Figures 3 through 5 show that the RMS error is a useful indicator of the quality of the correction. For example, for SWP2139 (Fig. 3) the quadratic correction looks best. It also has the lowest RMS. The Gaussian correction looks worst and has the largest RMS. The 3 Agency correction is intermediate in both appearance and RMS error. The quadratic correction also appears to be best for SWP4006 (Fig. 4). It has the lowest RMS for that spectrum, 2.1%, which is intermediate between SWP2139's 3 Agency and Gaussian correction. In appearance, the quality of the quadratic correction of SWP4006 is comparable with the 3 Agency correction of SWP2139. An inspection of the RMS errors reported in Table 1 indicates that the quality of the correction of the Quadratic algorithm is generally best.

A second comparison of the accuracy of the correction algorithms was made from line fluxes for emission line sources. Net line fluxes were calculated for the corrected spectra which originally had been processed with the bad ITF. These were then compared with the line fluxes that had been derived in the same manner from the same spectra processed with the good ITF.

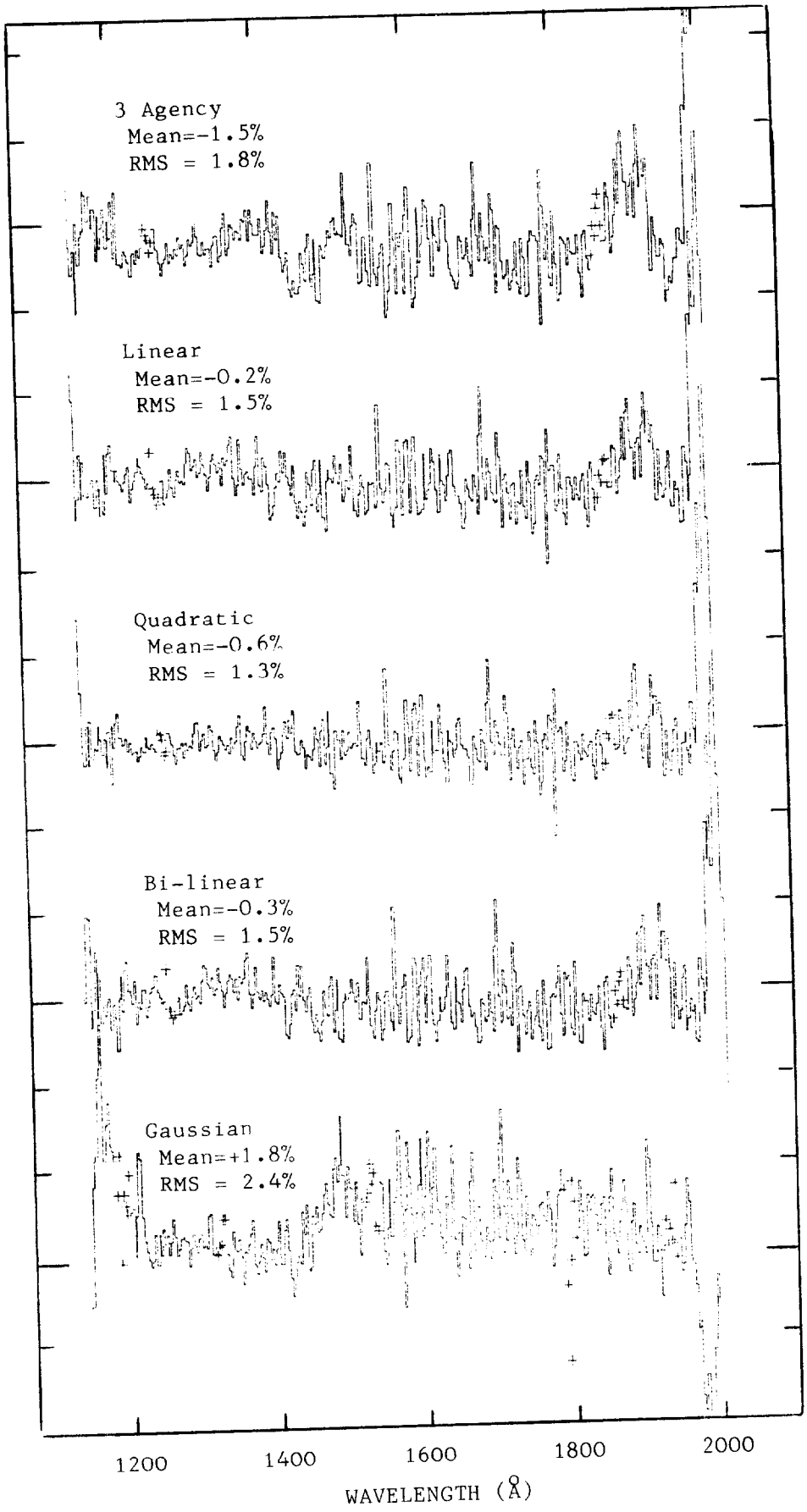

Fig.3- A comparison of the correction errors of the different algorithms on the spectrum of BD+28°4211 from image SWP2139.

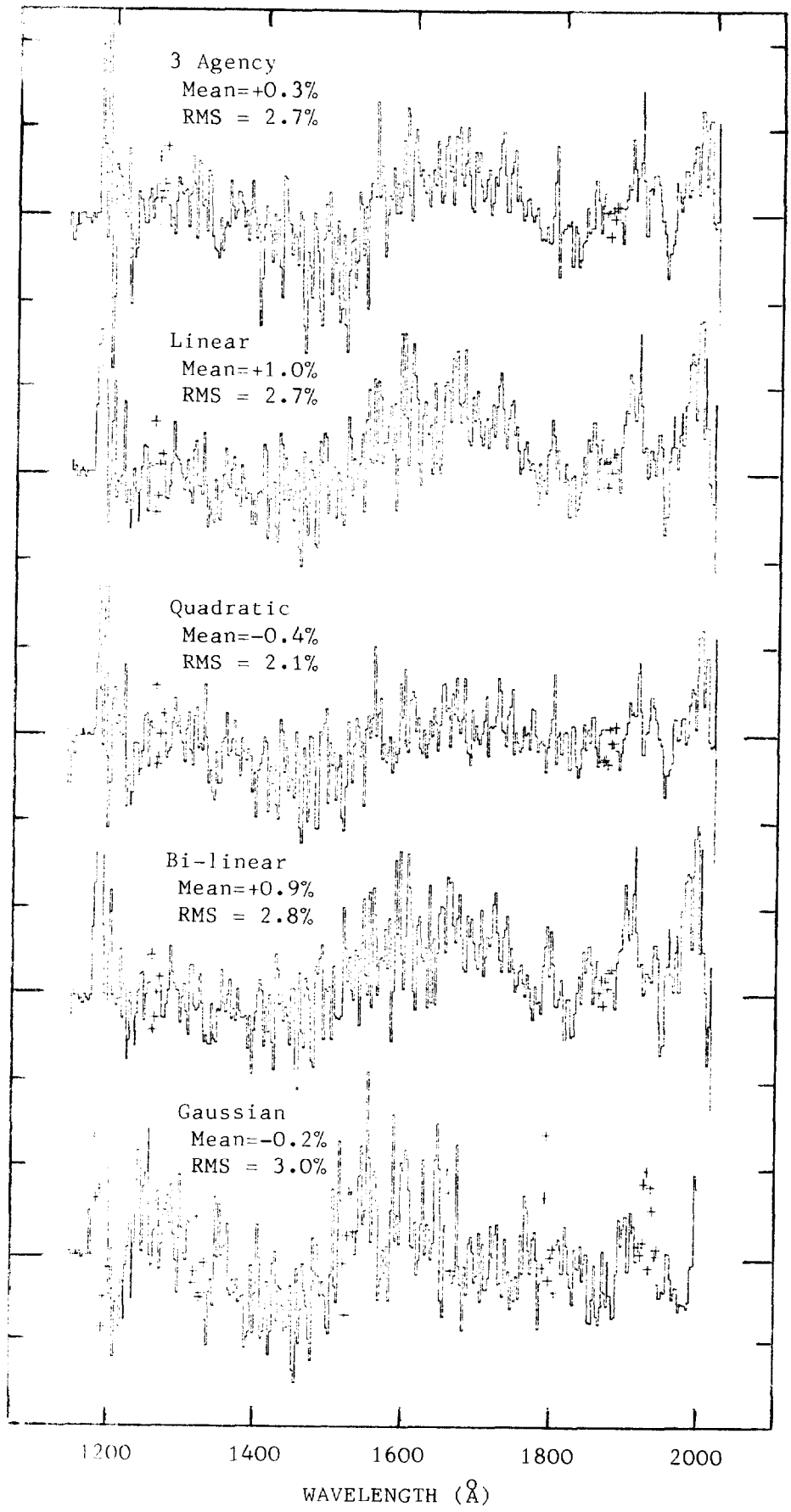

Fig.4- A comparison of the correction errors of the different algorithms on the spectrum of BD+33°2642 from image SWP4006.

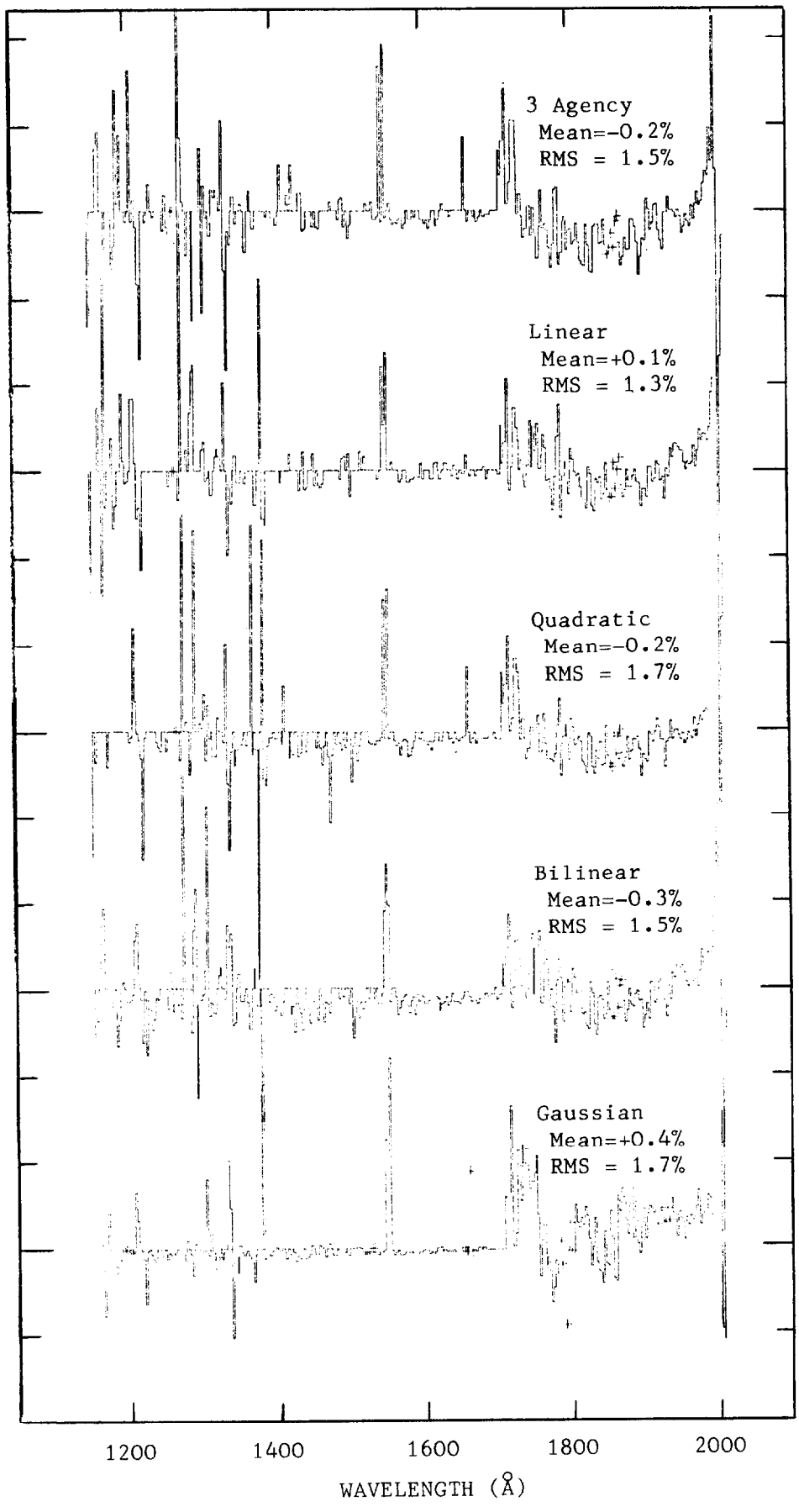

Fig.5- A comparison of the correction errors of the different algorithms on the spectrum of Capella from the image SWP4626.

TABLE 3

THE ACCURACY OF CORRECTED EMISSION LINE FLUXES

TARGET	IMAGE	WAVELENGTH	NET FN	CORRECTION ERRORS			
				3 AGENCY	LINEAR	BI-LINEAR	GAUSSIAN
Capella	SWP4626	1216 Å	147010	-1.7%	-1.6%	-0.7%	+0.1%
		1240	4980	-0.5	-0.2	-0.3	-0.0
		1306	28850	-0.7	+0.7	+3.5	+1.0
		1335	20760	-4.3	-1.2	+2.9	+2.9
		1550	18210	+5.1	+5.0	+6.1	+6.8
Nova Cyg	SWP3886	1240	84420	-2.7	-2.1	-2.1	-
		1335	15520	+2.3	+0.7	-0.9	-
		1400	20710	+2.0	+0.4	-0.9	-
		1486	72330	-1.6	-1.4	-0.5	-
		1550	105560	-1.1	-0.2	+0.0	-
		1640	4210	-1.8	-1.8	-2.3	-
		1750	110490	-4.6	-3.0	-3.5	-
		1909	154670	-0.3	+0.2	-0.2	-
⟨|ERRORS|⟩				2.0	1.3	1.7	2.2

Table 3 summarizes these comparisons. The errors added by the Linear algorithm are lowest, being only 60% of those added by 3 Agency algorithm. For the 3 Agency, Linear, and Bi-linear algorithms, the line fluxes for both the corrected and the correctly processed spectra were derived from the essr file. It should be noted that differences of up to ten percent have been found between line fluxes derived from the essr file and those derived from the eslo file. At this time we are not ready to offer any judgement concerning the relative photometric accuracy of data from the two files.

A comparison also was made of the amount of computer time required by the different algorithms. The Linear and Quadratic algorithms required 70% more time than the 3 Agency algorithm. The Bi-linear required 120% as much time as the 3 Agency. The Gaussian needed only 30% as much time as the 3 Agency when the latter processed the entire essr file. If only those orders from which the spectrum is extracted were processed, the two algorithms would run in about the same length of time.

IV. Conclusions

The data in Table 1 and Table 2 show that there is no algorithm which is always better than the others. Nor is there one which is always worse. The averages of the correction errors for each algorithm given in Table 4 show, nonetheless, that for point source spectra the Quadratic correction is usually best. The Gaussian algorithm is usually worst. For the extended sources, the averaged

TABLE 4

AVERAGED ERRORS FROM TABLES 1 AND 2

ALGORITHM	POINT SOURCES		EXTENDED SOURCES	
	MEAN	RMS	MEAN	RMS
3 Agency	0.9	2.6	0.5	1.8
Linear	0.6	2.3	0.4	1.7
Quadratic	0.7	2.2	0.4	1.8
Bi-linear	0.7	2.4	0.4	1.6
Gaussian	1.0	3.0	-	-

errors are much lower than those of the point source spectra and there is little difference in the accuracy of the five algorithms. This is as expected because many adjacent pixels will have nearly the same intensity in extended source spectra. Therefore, the little cleverness is needed to recover the original pixel values.

The correction errors added by all the algorithms were smaller than the reported intrinsic errors (col. 5 & 6 of Table 1). These intrinsic errors were determined by comparison with a single well-exposed, low background spectrum of the same star. Since there will be errors in these comparison spectra, the numbers given here actually represent upper limits to the intrinsic photometric errors for each spectrum when correctly processed with the good ITF. We estimated the errors in the comparison spectra by assuming they were half the mean errors and $1/\sqrt{2}$ the RMS errors that were given for 100% spectra in Table 3 of Cassatella et al. In this case, the errors introduced by the correction algorithms remained smaller than the re-estimated intrinsic errors.

Surprisingly the Bi-Linear decomposition was not the best for emission line fluxes. Since emission line intensities vary rapidly both along the dispersion and perpendicular to it, one would expect the Bi-Linear algorithm, which allows variation in both directions, to be best. The Bi-Linear average errors are affected by the large errors for the 1306 Å and 1335 Å Lines of Capella. However, even if these lines are excluded, the averaged errors for the Linear algorithm is still lower than those for the Bi-Linear.

Finally, as noted before, the Gaussian algorithm can be applied to high dispersion spectra if the appropriate flux transformations and order widths are used. We have experimented with correcting a few high dispersion orders.

These test corrections appear to be of the same order of quality as the low dispersion corrections of the Gaussian correction.

A. V. Holm
F. H. Schiffer, III

References

Cassatella, A., and Ponz, D. 1979, Report given at the IUE 3 Agency Coordination Meeting, VILSPA, Nov. 1979.
Cassatella, A., Holm, A.V., Ponz, D., and Schiffer, F. H., III, 1980, NASA IUE Newsletter, No. 8
Koornneef, J., and deBoer, K. 1979, NASA IUE Newsletter, No. 5.
Koornneef, J. 1979, private communication.